A&A 383, 30–45 (2002)
DOI: 10.1051/0004-6361:20011699

Astronomy & Astrophysics

New $UBVRI$ colour distributions in E-type galaxies

I. The data⋆,⋆⋆

T. P. Idiart[1], R. Michard[2], and J. A. de Freitas Pacheco[3]

[1] Instituto de Astronomia, Geofisica e Ciências Atmosféricas, Depto. de Astronomia, Universidade de São Paulo, Av. Miguel Stefano, 4200-CEP, 04301-904 S. Paulo, SP-Brazil
e-mail: thais@iagusp.usp.br
[2] Observatoire de Paris, LERMA, 77 Av. Denfert-Rochereau, 75015 Paris, France
e-mail: Raymond.Michard@obspm.fr
[3] Observatoire de la Côte d'Azur, Département Augustin Fresnel, BP 4229, 06304 Nice Cedex 4, France
e-mail: pacheco@obs-nice.fr

Received 17 September 2001 / Accepted 7 November 2001

Abstract. New colour distributions have been derived from wide field $UBVRI$ frames for 36 northern bright elliptical galaxies and a few lenticulars. The classical linear representations of colours against $\log r$ were derived, with some improvements in the accuracy of the zero point colours and of the gradients. The radial range of significant measurements was enlarged both towards the galaxy center and towards the outskirts of each object. Thus, the "central colours", integrated within a radius of $3''$, and the "outermost colours" averaged near the $\mu_V = 24$ surface brightness could also be obtained. Some typical deviations of colour profiles from linearity are described. Colour-colour relations of interest are presented. Very tight correlations are found between the $U-V$ colour and the Mg_2 line-index, measured either at the Galaxian center or at the effective radius.

Key words. galaxies: elliptical and lenticulars, CD – galaxies: ISM

1. Introduction

The "classical" data on the large scale colour distributions of E-type galaxies relies on observations by Bender & Möllenhof (1987), Vigroux et al. (1988), Franx et al. (1989), Peletier et al. (1990), Goudfrooij et al. (1994), to quote only the papers discussing the 1-D profiles of colour against radius, as distinguished from studies of dust patterns. Most of these data were reconsidered by Michard (2000) (RM00), in an attempt to collect a significant sample of objects with a complete optical colour set, i.e. $U-B$, $B-V$, $B-R$ and $V-I$ in a coherent photometric system. This was adequate to confirm previous indications about the cause of colour gradients: these appear to be due essentially to population gradients within galaxies, with the dust playing no important role, except in galaxies with central intense dust patterns. Such objects are rather rare among the Es.

Similar to most spectral indices of stellar populations, the colours suffer from the well known age-metallicity degeneracy, and, except $U-B$ or $U-V$, are not very sensitive to the two parameters. They are affected by dust, at least locally, or perhaps systematically in the central regions according to inferences based on a survey by Michard (1999) (RM99). On the other hand, they may be measured at lower surface brightnesses or larger radii than the line indices. They could therefore bring useful information to the study of fossil stellar populations, and further constraints upon models of the evolution of E galaxies. The present work aims to provide an enlarged sample of objects with complete colour data, extending farther in radius than in previous studies, and hopefully of improved accuracy.

In Paper I, we present the usual information about the observations and data reduction, and part of the results in tabular form. A larger set of results will be made available in electronic form. The frames, partly reduced, will be made available from the HYPERCAT database, Observatoire de Lyon.

Send offprint requests to: R. Michard,
e-mail: michard@obspm.fr

⋆ Based in part on observations collected at the Observatoire de Haute-Provence.

⋆⋆ Tables 9–11 plus detailed tables for each object are available in electronic form at the CDS via anonymous ftp to cdsarc.u-strasbg.fr (130.79.128.5) or via http://cdsweb.u-strasbg.fr/cgi-bin/qcat?J/A+A/383/30

In Paper II, under the assumption that the observed colour gradients reflect abundance variations along the radius, metallicity gradients will be computed from the present data, using new colour-metallicity calibrations derived from multi-population models for E-galaxies. These metallicity gradients allow an estimation of central and mean metallicities. Statistics of galaxies included in our sample indicate that mean metallicities are about solar, in agreement with the study by Trager et al. (2000) based on spectral indices.

Often used notations

- r isophotal radius; $r = (ab)^{1/2}$ for an ellipse of semi-axis a and b;
- Δ_{UB} colour gradient in $U - B$; $\Delta_{UB} = \mathrm{d}(U - B)/\mathrm{d}(\log r)$ and similar for other colours;
- diE, boE, unE: subclassification of E galaxies as disky, boxy and undetermined.

2. Observations

The observations were performed with the 120 cm Newtonian telescope of the Observatoire de Haute-Provence, in three runs: April 1–11 2000, May 29–June 5 2000 and January 18–29 2001, noted below as *run 1, 2 and 3*. Tables 1 to 4 gives lists of the observed galaxies with some parameters relevant on the observing conditions. A CCD target Tek1024 is mounted in the camera, giving a field of view of $11.6 \times 11.6'$ for a pixel size of 24 microns or $0.68''$. The relatively large field is a favorable feature of this system for the observation of colour distributions in nearby galaxies. Less favourable are the rather poor seeing at the OHP, with the $FWHM$ of star images usually in the 2–3$''$ range, with values at 4 or more during periods of northern wind (mistral), and also the sky illumination by ever increasing urban lights.

The camera is unfortunately affected by the so-called "red-halo" effect.

3. Data analysis

3.1. Outline of the operations

The analysis of the frames entails the following steps:

1. The usual corrections for offset, the "flat-fielding", and the interpolation of bad columns. As explained below we tried to improve the flat-fields by ad hoc "superflats";
2. The registration of the 5 frames in each passband to a common geometry, based on a set of measured coordinates for 6 to 12 stars. This is intended to simplify the derivation of colour maps if needed;
3. The preparation of each frame for measurement, involving a final attempt to measure and correct residual large scale background trends, corrections for parasitic objects, a treatment against cosmic rays peaks, and the calibration against the available results of aperture photometry (see Sect. 3.2.3);

Table 1. A list of the observations. The dates refer to the begining of the night. Two values W_o and W_i are given for the frame $FWHM$ (in $''$): the first is the original one; the second was attained after the treatment tending to equalize the $FWHM$ of all 5 frames in a colour set, this at the value of the best one. Notes: 2974 mistral, interfering bright star; 3115 mistral; 3193 interfering bright star; 3605 mistral, 3607 also observed; 3608 NGC 3607 interfering.

NGC	Date	F	File	Exp	Sky	W_o	W_i
2768	01/04/00	U	t613	3000	21.50	2.32	2.14
id	id	B	t614	600	21.71	2.22	2.11
id	id	V	t615	300	20.59	2.14	-
id	id	R	t616	240	19.93	2.29	2.14
id	id	i	t617	240	18.86	2.36	2.15
2974	05/04/00	U	t828	3000	20.75	5.10	4.10
id	id	B	t830	600	21.47	4.63	4.05
id	id	V	t829	300	20.54	4.04	-
id	id	R	t831	240	20.11	4.58	-
id	id	i	t832	240	18.47	4.23	-
3115	20/01/01	U	p437	2400	20.45	5.28	3.96
id	id	B	p438	600	21.35	4.12	3.74
id	id	V	p439	300	20.44	3.81	-
id	id	R	p440	200	19.93	3.86	-
id	id	i	p441	160	18.74	3.78	-
3193	01/04/00	U	t619	3000	21.09	3.11	-
id	id	B	t620	600	21.60	3.23	-
id	id	V	t621	300	20.78	3.26	-
id	id	R	t622	240	20.03	2.90	-
id	id	i	t623	240	19.27	2.75	-
3377	20/01/01	U	p443	2300	21.10	3.64	2.81
id	id	B	p444	600	21.72	3.02	2.69
id	id	V	p445	300	20.72	2.73	-
id	id	R	p446	200	20.16	2.80	-
id	id	i	p447	160	18.85	2.76	-
3377	27/01/01	U	p674	2500	20.73	3.62	2.75
id	id	B	p675	600	21.45	2.96	2.67
id	id	V	p676	250	20.47	2.70	-
id	id	R	p677	160	29.96	2.78	-
id	id	i	p678	130	18.68	2.71	-
3379	20/01/01	U	p449	2500	21.28	3.96	2.90
id	id	B	p450	600	21.86	3.29	2.84
id	id	V	p451	250	20.89	2.91	-
id	id	R	p452	160	20.32	3.11	-
id	id	i	p453	130	19.07	2.99	-
3605	05/04/00	U	t842	3000	21.16	4.62	4.05
id	id	B	t843	600	21.73	4.13	-
id	id	V	t844	300	20.76	3.93	-
id	id	R	t845	240	20.35	3.78	-
id	id	i	t846	240	19.35	3.88	-
3608	06/04/00	U	t937	3000	21.04	3.44	2.71
id	id	B	t938	600	21.77	2.90	2.71
id	id	V	t939	300	20.79	2.82	2.67
id	id	R	t940	240	20.29	2.79	2.74
id	id	i	t941	240	19.25	2.69	-
3610	20/01/01	U	p456	2500	21.39	2.99	2.49
id	id	B	p457	600	21.99	3.11	2.51
id	id	V	p458	250	21.07	2.71	2.44
id	id	R	p459	160	20.49	2.51	-
id	id	i	p460	130	19.21	2.75	2.43

Table 2. A list of the observations (continued). See conventions above. Notes: 4125 clouds; 4278 NGC 4283 also observed; 4387 mistral; 4406 (30/5) clouds; 4406 (31/5) mistral.

3613	20/01/01	U	p462	2500	21.25	3.58	2.43
id	id	B	p463	600	21.92	3.16	2.25
id	id	V	p464	250	20.90	2.42	2.11
id	id	R	p465	160	20.26	2.16	-
id	id	i	p466	130	19.03	2.20	-
3640	07/04/00	U	t040	3000	20.68	3.00	2.14
id	id	B	t041	600	21.27	2.29	2.14
id	id	V	t042	300	20.40	2.14	-
id	id	R	t043	240	20.04	2.22	2.18
id	id	i	t044	240	19.06	2.26	2.09
3872	06/04/00	U	t953	3000	21.03	2.89	2.36
id	id	B	t954	600	21.68	2.49	2.43
id	id	V	t955	300	20.70	2.38	-
id	id	R	t956	240	20.17	2.49	2.37
id	id	i	t957	240	19.18	2.67	2.43
4125	21/01/01	U	p521	2500	20.07	2.13	1.93
id	id	B	p522	720	21.08	2.14	1.94
id	id	V	p523	420	19.85	1.97	-
id	id	R	p524	280	18.47	2.48	1.98
id	id	i	p525	250	17.40	2.11	2.00
4261	21/01/01	U	p527	2500	20.05	2.84	2.39
id	id	B	p528	720	21.10	2.61	2.40
id	id	V	p529	420	20.25	2.41	-
id	id	R	p530	280	20.07	2.61	2.50
id	id	i	p531	250	18.78	2.53	2.52
4278	25/01/01	U	p600	2500	20.96	3.20	2.93
id	id	B	p601	600	22.03	2.89	-
id	id	V	p602	250	21.10	3.54	2.96
id	id	R	p603	160	20.33	3.60	2.98
id	id	i	p604	130	19.05	3.23	2.86
4365	25/01/01	U	p606	2500	20.72	3.52	2.93
id	id	B	p607	600	21.75	3.39	2.95
id	id	V	p608	250	20.74	2.99	-
id	id	R	p609	160	20.01	3.17	2.94
id	id	i	p610	130	18.64	2.82	-
4374	01/04/00	U	t629	3000	21.20	3.08	-
id	id	B	t630	600	21.84	3.20	-
id	id	V	t631	300	20.85	3.05	-
id	id	R	t632	240	20.36	2.94	-
id	id	i	t633	240	19.32	2.85	-
4387	05/04/00	U	t856	3000	21.23	4.40	-
id	id	B	t857	600	21.79	4.35	-
id	id	V	t858	300	20.77	4.08	-
id	id	R	t859	240	20.35	4.23	-
id	id	i	t860	240	19.35	4.19	-
4406	30/05/00	U	m606	2400	20.06	2.65	2.14
id	id	B	m607	600	20.69	2.69	2.19
id	id	V	m608	300	19.21	2.65	2.12
id	id	R	m609	150	17.76	2.39	2.09
id	id	i	m610	120	17.28	2.09	-
4406	31/05/00	U	m616	2400	20.42	4.66	2.14
id	id	B	m617	500	20.50	4.27	2.19
id	id	V	m618	250	19.24	4.32	2.12
id	id	R	m619	180	19.08	4.14	2.09
id	id	i	m620	150	18.16	3.85	2.09

Table 3. A list of the observations (continued). See conventions above. Notes: 4551 NGC 4550 also observed; 4552 clouds.

4472	07/04/00	U	t053	3000	20.98	2.43	2.29
id	id	B	t054	600	21.53	2.49	2.30
id	id	V	t055	300	20.60	2.24	-
id	id	R	t056	120	20.16	2.37	-
id	id	i	t057	120	19.09	2.32	-
4473	29/05/00	U	m571	2700	20.73	2.88	-
id	id	B	m572	600	21.61	3.01	-
id	id	V	m573	300	20.70	2.99	-
id	id	R	m574	180	20.22	2.99	-
id	id	i	m575	150	18.99	2.88	-
4478	25/01/01	U	p600	2500	21.00	3.56	2.58
id	id	B	p601	600	21.59	3.64	2.65
id	id	V	p602	250	20.62	3.12	2.48
id	id	R	p603	160	19.92	3.11	2.54
id	id	i	p604	130	18.62	2.52	2.86
4486	27/01/01	U	p680	2500	20.86	4.35	3.67
id	id	B	p681	600	21.67	3.98	3.59
id	id	V	p682	250	20.70	3.92	3.71
id	id	R	p683	160	20.15	4.03	3.72
id	id	i	p684	130	18.92	3.62	-
4494	05/04/00	U	t871	3000	21.18	3.62	3.30
id	id	B	t872	600	21.66	3.31	-
id	id	V	t873	300	20.56	3.47	-
id	id	R	t874	240	20.04	3.47	-
id	id	i	t875	240	18.92	3.26	-
4551	01/06/00	U	m647	2400	20.69	2.48	2.16
id	id	B	m648	500	21.44	2.58	2.15
id	id	V	m649	250	20.59	2.40	2.19
id	id	R	m650	180	20.33	2.16	-
id	id	i	m651	150	19.43	2.28	2.13
4552	02/06/00	U	m693	2400	19.67	2.92	2.49
id	id	B	m694	500	21.16	2.79	2.48
id	id	V	m695	250	20.26	2.50	-
id	id	R	m696	180	19.90	2.82	2.51
id	id	i	m697	150	18.96	2.99	2.50
4564	27/01/01	U	p686	2500	20.86	3.92	3.41
id	id	B	p687	600	21.59	3.44	-
id	id	V	p688	250	20.70	3.56	-
id	id	R	p689	160	20.00	3.85	3.47
id	id	i	p690	130	18.62	3.53	-
4621	06/04/00	U	t966	3000	20.75	2.85	-
id	id	B	t967	600	21.50	2.81	-
id	id	V	t968	300	20.39	3.05	2.77
id	id	R	t971	120	19.68	2.82	-
id	id	i	t972	120	19.24	2.88	-
4636	27/01/01	U	p693	2263	20.68	3.86	3.11
id	id	B	p694	662	20.78	3.61	3.06
id	id	V	p695	300	20.25	3.35	2.99
id	id	R	p696	210	19.47	3.47	2.99
id	id	i	p697	180	18.22	3.05	-
4649	03/06/00	U	m723	2400	20.15	2.57	-
id	id	B	m724	500	21.20	2.62	-
id	id	V	m725	250	20.18	2.52	-
id	id	R	m726	180	19.82	2.52	-
id	id	i	m727	150	18.80	2.34	-

Table 4. A list of the observations (continued). See conventions above. Notes: 5831 mistral and clouds.

5322	06/04/00	U	t992	3000	20.95	2.91	2.52
id	id	B	t993	600	21.72	2.64	2.64
id	07/04/00	V	t994	300	20.69	2.93	2.53
id	id	R	t080	240	20.62	1.80	2.51
id	id	i	t081	240	19.49	1.87	2.51
5576	07/04/00	U	t083	3000	20.73	2.31	-
id	id	B	t084	600	21.22	2.52	2.31
id	id	V	t085	300	20.38	2.67	2.30
id	id	R	t086	240	19.87	2.48	2.26
id	id	i	t087	240	18.79	2.39	-
5813	29/05/00	U	m579	2400	20.95	3.47	3.18
id	id	B	m580	500	21.66	3.28	3.18
id	id	V	m581	250	20.71	3.19	-
id	id	R	m582	180	20.28	3.09	-
id	id	i	m583	150	19.13	3.16	-
5831	31/05/00	U	m622	2400	20.43	3.89	3.28
id	id	B	m623	500	20.66	4.07	3.28
id	id	V	m624	250	18.84	3.33	-
id	id	R	m625	180	18.06	3.23	-
id	id	i	m626	150	16.73	3.19	-
5846	01/06/00	U	m654	2400	20.66	2.55	2.11
id	id	B	m655	500	21.28	2.74	2.16
id	id	V	m656	250	20.38	2.07	-
id	id	R	m657	180	20.08	2.28	2.11
id	id	i	m658	150	19.08	2.33	2.11
5866	02/06/00	U	m700	2400	21.16	2.43	1.93
id	id	B	m701	500	21.76	2.26	1.88
id	id	V	m702	250	20.80	1.84	-
id	id	R	m703	180	20.36	1.91	-
id	id	i	m704	150	19.37	1.82	-
5982	03/06/00	U	m730	2400	20.89	2.20	2.00
id	id	B	m731	500	21.15	2.30	2.06
id	id	V	m732	250	20.46	2.07	-
id	id	R	m733	180	20.18	2.11	-
id	id	i	m734	150	19.13	2.33	2.06

4. Large errors in colour measurements may result from small differences between the widths of the PSFs of the two frames involved (see for instance Michard 1999, and the previous literature quoted therein). When the $FWHM$s of measured PSFs in the colour set for a given object differed by more than 10%, it was our practice to modify the frame PSFs and try to make them equal to that of the best frame of the group (see Sect. 3.2.4);
5. The isophotal analysis of the V frame was performed according to Carter (1978), as implemented in the Nice technique described in Michard & Marchal (1994) (MM94);
6. The correction procedures for the red halo effect in $V - I$, and eventually for the effects of different PSF far wings in other colours, were performed (see Sect. 3.2.5). The correction necessitates the crossed correlation of the V frame by the I PSF and conversely. This operation cancels out the errors in the colour distribution induced by the red halo, but degrades the resolution. A correction to the calibrations performed before the convolutions is needed;
7. Finally, colour measurements were performed along the previously found isophotal contours, and the average isophotal colours tabulated. Our routine at this stage involves corrections to the adopted values of the sky backgrounds, in order to eliminate the obvious effects of inaccuracies in these (see Sect. 3.2.6);
8. The V surface brightness and colours have been collected in ad hoc files, and corrected for galactic absorption (or reddening) and the K effect, according to the precepts and constants given in the Third Reference Catalogue of Bright Galaxies (RC3, de Vaucouleurs et al. 1991). The usual linear representation of colours against $\log r$ have been calculated *in selected ranges*, avoiding on the one hand the central regions affected by imperfect seeing corrections and/or by important dust patterns; and on the other the outer range presumably affected by poor background corrections and residual noise.

Table 5. Measurements of residual fluctuations in background before and after the final "rectification". Unit: % of sky background.

Colour	U	B	V	R	i
Flats+superflats 1st run	1.84	1.19	0.72	0.68	0.95
id. 2nd run	1.90	0.77	0.45	0.54	0.79
id. 3rd run	0.69	0.79	0.56	0.60	0.64
Final treatment 1st run	0.36	0.34	0.30	0.29	0.28
id. 2nd run	0.40	0.27	0.26	0.31	0.30
id. 3rd run	0.28	0.28	0.24	0.20	0.32

3.2. Detail of operations

Some important details of the above summarized procedures will now be discussed.

3.2.1. The background

The sky background of flat-fielded frames showed disappointingly *large scale trends*, specially in the U band. To improve upon this situation, it was tried to derive corrections by mapping the background of such frames, at least those which were not "filled" by a large galaxy. Such maps were found to be correlated, although less so than expected, and their average used as a "superflat". The quality of the background was then generally improved: if not, the superflats were not used. Note that, in the observing runs of May 2000 and January 2001, a number of frames of "empty" fields were obtained (sometimes in moonlight hours) to contribute to the derivation of superflats.

A final improvement was obtained by measuring, during the treatment of each frame, a number of background patches, and subtracting a linearly interpolated map of these, instead of a constant. The background residual *large scale* fluctuations were often measured at the three steps

of the procedure, that is, after the application of the flats, of the superflats, and after the final treatment. Table 5 summarizes the results. It may be noted that the combination of flats and superflats left large errors in our first and second runs, specially in the U colour. The final background linear "rectification" allowed quite significant improvements, as seen by comparing the upper and lower halves of the table.

If we consider an E galaxy observed under the typical conditions of the present series (see above for a tabulation of sky background values), the final residual fluctuations quoted here represent *local errors* of less than 0.1 mag near the isophote $\mu_B = 25$. We will return later to the question of errors resulting from background uncertainties.

3.2.2. Parasitic objects

In galaxy photometry it is necessary to remove parasitic objects, stars and galaxies, that overlap the measured object. In the present work we used concurrently the following techniques:

- replacement of pixels in a circle enclosing the "parasite" by a circle symmetric about the center of the galaxy;
- replacement of the circle by another one chosen in a nearby area;
- marking of the pixels to be discarded in such a way that they are later left aside in the measuring programmes.

3.2.3. Calibrations

The frames were calibrated by comparisons with the results of aperture photometry. Our first choice was to use the $UBVRI$ data of Poulain (1988) (PP88), Poulain & Nieto (1994) (PN94) that are available for 26 objects of our survey, and are in Cousins's system, notably for R and I. In a few cases the data collected in the HYPERCAT catalogues were used. These contain both primary data (those with an independent photometric calibration), and secondary data (actually calibrated with part of the primary data). Only primary data were used, selected according to our previous experience or prejudices. A few completely missing calibrations in R and I were replaced by values calculated from the tight correlations of $V - R$ and $V - I$ with $B - V$, derived from Poulain's data for E galaxies.

Although the I filter in the camera is of Gunn's type, our photometry is transfered to Cousins's system through the calibration. It is assumed that the difference of pass-bands has no significant effect on colour gradients.

3.2.4. Equalization of PSF *FWHM*'s

Many studies of colour distribution in galaxies are affected by errors resulting from the difference in the PSFs of the two frames involved in a colour measurement. Franx et al. (1989), Peletier et al. (1990), Goudfrooij et al. (1994) calculated the radial range where the errors due to "differential seeing" are larger than some accepted threshold, and discarded the corresponding colours. Our policy, for instance in RM99, was to correct for this effect by adjusting the two frames to have PSFs with a common $FWHM$.

In the present study we tried to equalize the PSFs of the 5 frames in a given colour set. This is feasible if the 5 frames are taken in rapid succession, so that the PSFs have similar widths. The frame with the narrowest PSF is selected, and we find by trial and error a narrow Gaussian (or sum of two Gaussians) which can restore another frame to the same quality, or rather the same $FWHM$, by deconvolution. The parameters at hand are the σ of the Gaussian and the number of iterations in the deconvolution. In Tables 1 to 4 we give the original $FWHM$ $W_{\rm o}$ of each frame, and the improved $W_{\rm i}$ after the procedure described here. Obviously this cannot lead to perfect results, and sometimes we find in our data the signature of "differential seeing", in the form of *large* colour variations, peaks or dips, within the seeing disk: these defects were edited out unless there was some good reason to suspect a genuine central colour anomaly, such as large dust patterns, or the jet of NGC 4486.

The reader may notice that two observations of NGC 4406 are listed in Table 2, one of May 30, the other of May 31 2000. The first one was taken through fog and with average seeing, while for the other the "mistral" brought a clearer sky and very poor seeing. A special treatment was then applied: the central peak of the sharp images was "grafted" on the corresponding regions of the unsharp but deeper images. This explains why the $W_{\rm i}$ is so much narrower than the original $W_{\rm o}$ for the frames of May 31.

3.2.5. "Red halo" and PSFs far wings

Before the start of this survey, the CCD camera on the telescope used was known to be affected by the "red halo", an unfortunate property of thinned CCDs. The aureoles surrounding stellar images are obviously brighter and more extended in the I band than in B or V. Not only the red halo, but more generally the outermost wings of PSFs, were measured during our observing runs in 2000-1. The techniques and results are described in Michard (2001) (RM01). *The choice of appropriate star fields allowed us to extend the measurements up to a radius of nearly 3′, and down to a level of about* 0.5×10^{-6} *of the central peak.* Due to the red halo effect, PSF wings in I may be a factor of 3 brighter in an extended radius range than the V ones. Much smaller but still significant differences may also occur between the PSFs of various spectral bands, the V PSF wings always being fainter. The V PSF wings however, and all the others at the same time, were reinforced between our observing runs of spring 2000 and winter 2001, probably an effect of 10 months ageing of mirrors coatings. The final output of the measurements are average "synthetic" PSFs in the format 512×512 pixels, or $5.8 \times 5.8'$, for each run and pass-band.

Table 6. Comparisons of average color gradients for different subsamples of E galaxies, before or after tentative corrections for the effects of PSF far wings according to RM01. No corrections are applied if the average observed gradients are close to the adopted reference. N, number of objects. Δ_{U-B}, etc. mean gradients.

Subsample	N	Δ_{U-B}	σ	Δ_{B-V}	σ	Δ_{V-R}	σ	Δ_{V-I}	σ
RM00	29	−0.152	0.048	−0.061	0.025	−0.018	0.030	−0.053	0.022
2000 Observ.	23	−0.138	0.037	−0.064	0.018	+0.018	0.015	+0.093	0.047
2000 Correc.	23	−0.116	0.038	-	-	−0.016	0.013	−0.048	0.026
2001 Observ.	14	−0.174	0.045	−0.080	0.022	−0.017	0.013	+0.040	0.037
2001 Correc.	14	−0.140	0.036	-	-	-	-	−0.062	0.025

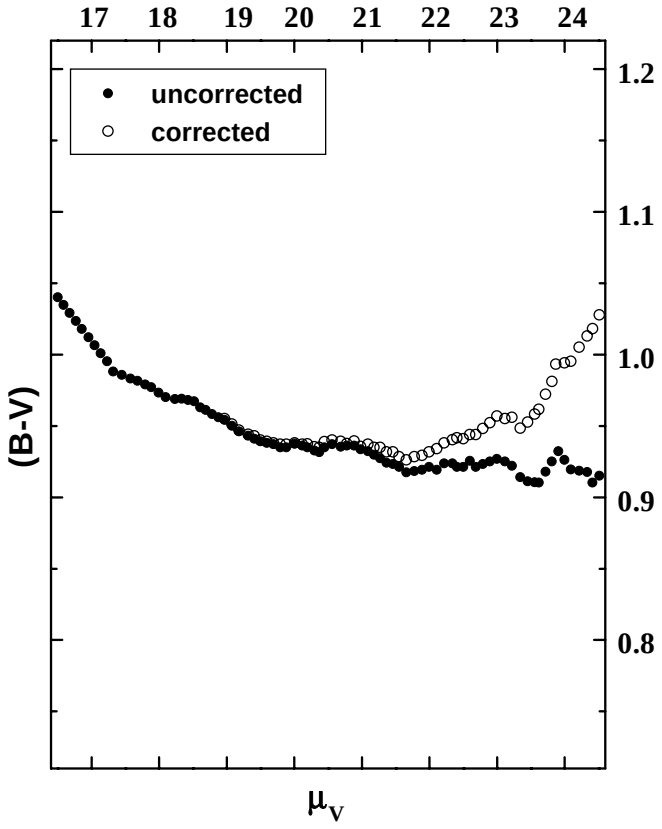

Fig. 1. Example of the "correction" of a colour profile through changes in the sky background constants. Abscissae: V surface brightness in mag. Ordinates: $B-V$. Uncorrected: open circles. Corrected: filled circles. The changes of the background amount here to −0.25% in B and 0.10% in V, that is more than average (see Table 7).

A set of numerical experiments on model galaxies is also presented in RM01, to illustrate the effects of these far wings on the observed surface brightness and colour distributions. The most striking effect occurs for the gradient Δ_{VI}, which appears strongly positive, while it is negative according to the classical results of Bender & Möllenhof (1987), or Goudfrooij et al. (1994). More subtle effects are found for other colours, with relatively small but definite changes in gradients.

To correct for the consequences of the red halo, or other similar effects upon the colour distribution in the index C1−C2, *frame C1 is convolved with the PSF of frame C2 and conversely.* After this operation, the resulting images have been submitted to the same set of convolutions, one in the atmosphere plus instrument, the other in the computer: they lead therefore to correct colour distributions, but with a significant loss of resolution. As the convolutions attenuate the central regions of the galaxy, and much more so for the V frame convolved by the I PSF, the mean colours are biased: a correction to the calibrations performed before the convolutions is needed. This has been done by a comparison of simulated aperture photometry to the observed one, an operation also used to estimate the errors in calibration (see below).

Since the extended PSFs are found with limited accuracy, it is necessary to discuss the validity of the corresponding corrections obtained through crossed convolutions, the more so because of the obvious changes of the PSF far wings between *run 1* and *run 3*. The mean values of the colour gradients for subsamples of E galaxies have been used for these checks, with the results of Table 6. For a subsample of 12 or more E galaxies the mean colour gradients and their dispersions cannot differ much, so that their values may be used as checks of the need for a correction and its eventual success[1]. The reference for these comparisons is the subsample in Michard (2000) (RM00), mostly a rediscussion of the "classical" data by Peletier et al. (1990), Goudfrooij et al. (1994) and others.

Looking at the Table 6, it is clear that the red halo introduces enormous errors in the $V-I$ gradients, but that the corrections are remarkably successful in restoring the agreement of the results with the accepted reference, both as regards the mean values and the dispersion. The same may be said about the $V-R$ gradients. The wings of the V PSF were strongly reinforced between our *run 3* and *run 1 or 2*, but much less so for the I and R PSF wings. As a result the red halo effect is less in $V-I$ for the frames of *run 3* and disappears in $V-R$.

The situation is less clear for the $U-B$ distributions. Our mean uncorrected gradients are in good agreement

[1] This assertion is questionable as pointed out by the referee. We therefore tested it by comparing the distributions of the gradients in subsamples of 15 to 25 objects, sorted out by NGC numbers, from the surveys of Peletier et al. (1990), Goudfrooij et al. (1994) and our discussion in RM00. This procures 8 tests, according to the number of colours in each of the sources. It turns out that the subsamples are statistically coincident in 4 cases. They differ by slightly more than the calculated errors in the others.

with the "classical" data, essentially from Peletier et al. (1990), as rediscussed in RM00. On the other hand, the U PSF wings are consistently above the V ones in all our runs, so that the true slopes of the $U-B$ variations may be a bit smaller than the observed ones. This error might well be present in the classical observations. Incidentally, the data of Peletier et al. were obtained in $U-R$, and it is impossible to be sure that the far PSF wings of the used telescope were the same in both pass-bands!

Similar remarks might be made about our $B-V$ data. Since the mean measured gradient is the same for our data of the year 2000 and the adopted reference (and as a good B PSF is not available) we take as correct this set of results. For our data of 2001, there is evidence that the wings of the B PSF were slightly above those of the V one, so that the $B-V$ gradients might also be biased upwards.

It appears that a significant source of error in the measurement of the small colour gradients in E galaxies has hitherto been overlooked. It might be that small systematic errors, of the order of some 15–20%, are still present in the U−B or U−V gradients published here. Although such errors would not have significant astrophysical implications, control observations are planned.

3.2.6. Measurements of isophotal colours

Our procedure uses Carter's isophotal representation of the V frame. The successive contours at 0.1 mag intervals are fitted to each of the two frames to be compared, the mean surface brigtnesses calculated and the corresponding magnitudes and colours derived. A sliding mean smoothing is applied to the data for the outer contours and a graph of the colour against $\log r$ displayed. This might hopefully be linear, or nearly so, in the studied range. If it is not, *it is our practice to introduce corrections to the provisional values of the sky background for one or both of the frames, in order to get rid of the "breaks" in the colour-radius relation typically associated with a poor choice of the background constant.* The reader is referred to the graphs published in Goudfrooij et al. (1994) for examples of such features. In Fig. 1 we show a color profile with a rather important defect due to poor backgrounds, and its adopted correction.

The introduction of such "aesthetic" corrections to the raw data might be criticized, since it assumes a regular behaviour of the colours at large $\log r$. This is however a reasonable hypothesis: the introduced corrections remain small, as shown by the statistics of Table 7. It should be noted that the *mean sky background values* derived for our large field frames are more precise than in previous works based on small field frames, where the sky was not reached at all. The problem lies in the presence of residual large-scale background fluctuations (see above): their effects are similar to those resulting from the poor evaluation of a constant background, and can be approximately corrected by the introduction of an ad hoc constant, or rather a set of constants, for the 5 frames in the colour set.

Table 7. Corrections to provisional sky background values applied to cancel out "breaks" in the run of colours aginst $\log r$. The table gives the mean absolute values of the applied corrections. Unit: % of sky background.

Colour	U	B	V	R	I
1st and 2nd run	0.22	0.14	0.12	0.18	0.20
3rd run	0.14	0.07	0.02	0.08	0.14

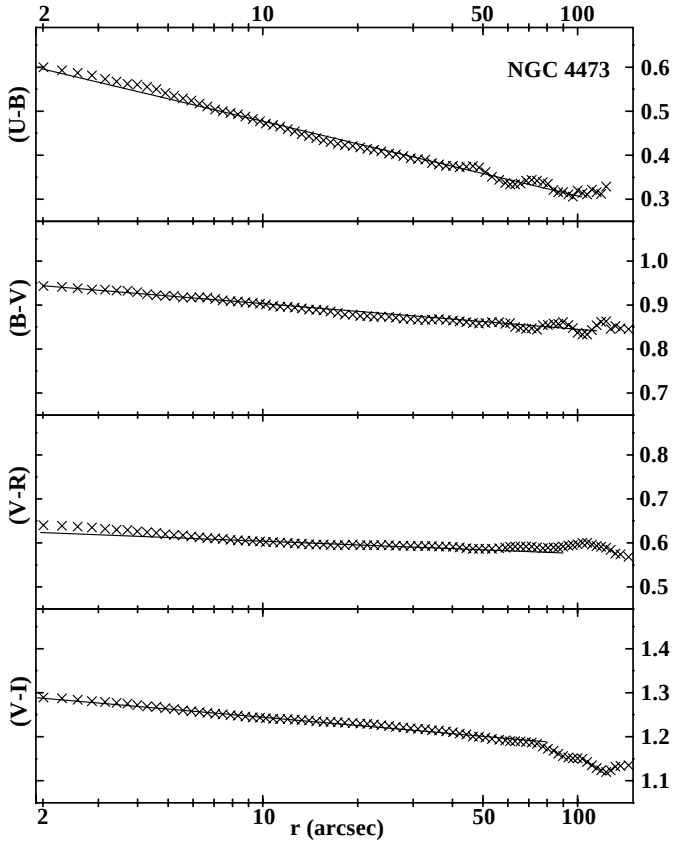

Fig. 2. Example of a set of "regular" colour profiles for NGC 4473. In this case, the colours are nearly linear in $\log r$ through the observed range. In this particular case a linear fit was made in the range 5–80″ to provide the tabulated data.

The linear fit was finally performed on a range of $\log r$ selected so as to avoid the central regions affected by known dust patterns or possible residual seeing-induced errors, and the outermost regions visibly affected by deviations from the expected straight line.

3.2.7. Errors

The noise is not a significant source of error in this type of work, because averages can be performed upon thousands of pixels in the galaxy regions of low S/N ratio. Residual noise effects at large r can be easily recognized in sample plots of the data (see Figs. 1–4). The main sources of errors lie:

– in the calibration, giving a probable error σ_C, affecting equally all parts of a given object, but dependent

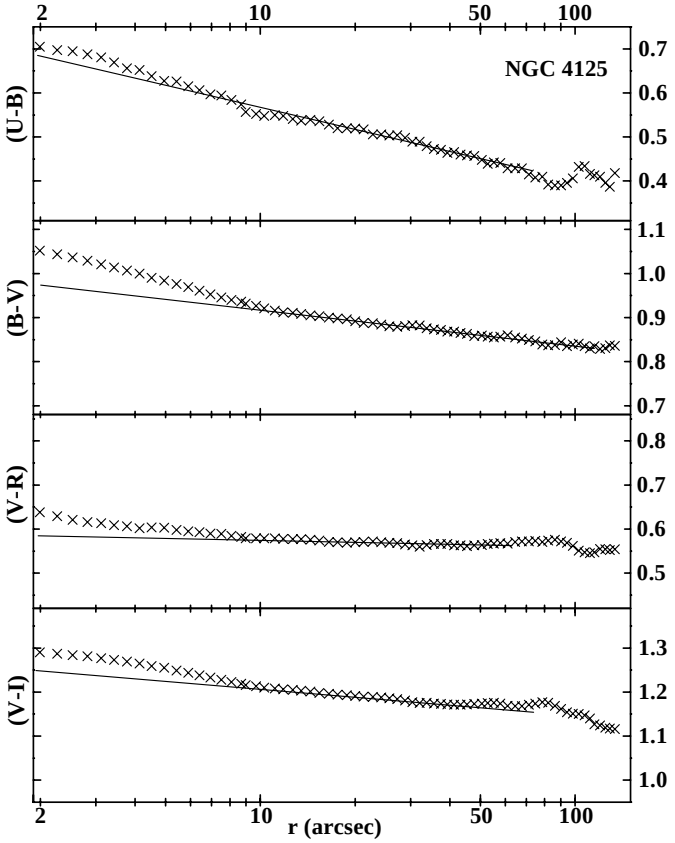

Fig. 3. Example of a set of colour profiles for NGC 4125, a galaxy with a central dust pattern of importance index 3. In this case, the colours show a hump for $r < 10''$, small in $U-B$ but much larger in other colours. In this case, the linear fit was restricted to the range 10–80″.

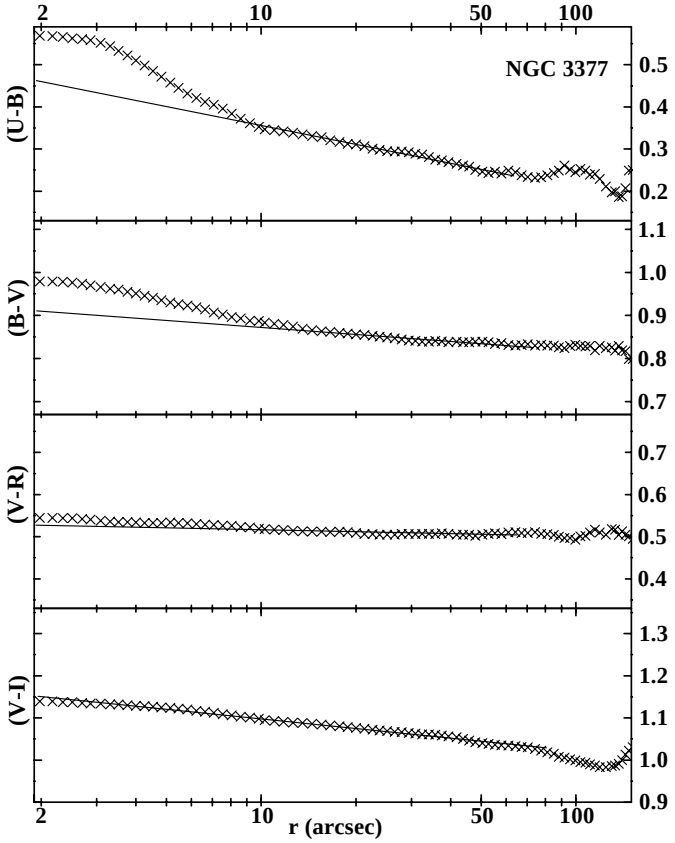

Fig. 4. Example of a set of colour profiles for NGC 3377, a galaxy with a central red hump in $U-B$ or $B-V$ but not in $V-I$. This suggests a metallicity effect. The fit was obtained in the range 8–80″.

upon the quality of the available aperture photometry in each colour;
- in the "differential seeing", i.e. the small differences in PSF between the frames in a colour set, also after the adjustments described above. This error σ_0 occurs only near the center of the objects, say in a diameter of twice the seeing $FWHM$ (it would be a much larger range without the performed adjustments). There is no obvious reason for it to be colour dependent;
- in the sky background residual large-scale fluctuations, or equivalently, errors in the sky background estimates. This error σ_S is strongly dependent upon colour and the studied radius, or rather the corresponding surface brightness.

These three components of the total error will now be considered, together with other relevant topics.

1. *Errors in colours from calibration inaccuracies.*
When a number of measurements are available for a given object, for instance 5 apertures in PP88 and PN94, a probable error of the resulting calibration is readily derived from the dispersion of these measured values about the results of simulated aperture photometry, calculated from our data, i.e. V magnitudes, isophotal parameters and colours. For the preferred calibrations with Poulain's data, the computed error is often less than 0.01 in $B-V$ or $V-R$ but may rise to 0.02 in $U-B$ or $V-I$. Still larger calibration errors, up to 0.04, have been estimated for objects with very scanty or uncertain aperture photometry. These probable errors apply to the zero point of the colour regression as shown in Table 9, and to all colour data from the same object.
2. *Residual errors from PSF equalization.*
The residual errors after this step in our data treatment can be objectively ascertained by comparing the "central" $B-R$ colours in our survey with the equivalent data from RM99, derived from high-resolution CFHT frames. For the present survey the "central colours" are the integrated colours within a radius of 3″. From RM99, Table 6, we find the colours at the isophote of 1.5″, which are likely similar. The statistics of the difference $B-R$(new)–$B-R$(RM99) are for 31 objects in common: mean = 0.01 $\sigma = 0.038$. Assuming then that the errors are equal in the two surveys, the probable error associated with poor PSF adjustements is $\sigma_0 = 0.027$ in $B-R$. This source of error has no reason to vary significantly from one colour to another. It is independent of the error of calibration previously discussed.

The comparison between the two surveys is made possible because the same set of calibrations has been used, although the field of the CFHT frames was often not sufficient to use all calibrations apertures. A minor part of the above differences may come from this source. In RM99, the $B-R$ of NGC 2768 is quoted too red by 0.08 and that of NGC 3610 too red by 0.10.

3. *Errors from sky background inaccuracies*
Given ϵ_A and ϵ_C, the relative errors in the sky background evaluation for frames A and C, A and C beeing a pair among $UBVRI$, the magnitude error in the colour $A-C$ may be expressed as $\delta_{A-C} = -2.5\log(1+\epsilon_A 10^{0.4\Delta\mu_A})+2.5\log(1+\epsilon_C 10^{0.4\Delta\mu_C})$. Here $\Delta\mu_A$ is the magnitude contrast between the object and the sky in colour A. Using average values for the colours of E-galaxies and for the sky brightnesses, $\Delta\mu_A$ for any colour may be expressed in terms of $\Delta\mu_V$. Then, in the range of small δ_{A-C}, the expression reduces to $\delta_{A-C} = 1.0857(K_A\epsilon_A - K_C\epsilon_C)10^{0.4\Delta\mu_V}$ where $K_A = 10^{0.4\Delta\mu_A}/10^{0.4\Delta\mu_V}$.
$K_V = 1$ by definition; we find $K_U = 3.1$ and $K_I = 1.55$, while K_B and K_R are slightly below 1.
The ϵ_A, ... are unknown, but it is feasible to get statistics of the linear combinations $K_A\epsilon_A - K_C\epsilon_C$. Indeed, as explained above, we have adopted ad hoc corrections to provisional sky background values, in order to regularise the colour-log r relations. It is reasonable to assume that the *errors left after these corrections are proportional to the adopted corrections themselves.* We take $\delta_{A-C} = \eta K_{AC} = \eta(K_A\epsilon_A - K_C\epsilon_C)$, where η is a small constant and the K_{AC} may be derived from the statistics of the adopted corrections given in Table 7. In practice somewhat different statistics have been calculated, to take into account the fact that our corrections for two colours are not necessarily uncorrelated. The constant η, different for our observing runs of 2000 and 2001, was chosen so as to get a system of errors compatible with the appearance of the data and also with the errors found for the slopes of the colour-log r relation. The finally adopted errors σ_S from sky background inaccuracies are given in Table 8. Note that this source of error is negligible for $\mu_V = 22$ or smaller. Predicted errors are reduced for our *run 3* as compared to the two others.

4. *Total errors*
The above estimated errors are independent and should be added quadratically. In the central region with $r < 6''$, the total error will be $\sigma_T = (\sigma_C^2 + \sigma_0^2)^{1/2}$. In the mean region with $18 < \mu_V < 22$ the total error equals the calibration error. Finally, in the outer range of $\mu_V > 23$ one can use $\sigma_T = (\sigma_C^2 + \sigma_S^2)^{1/2}$.

5. *Errors from the corrections for red halo and other far wings effects*
To our knowledge, the crossed convolutions used to correct for the red halo and similar effects do not give rise to random errors, but rather to systematic errors due to inaccuracies in the adopted PSFs. Such problems may be detected from the study of the distributions of the slopes of the colour-log r relations discussed below.

6. *Errors in the slopes of the colour*-log r *relations*
These have been calculated by two complementary methods. On the one hand, we can look for the correlations between the slopes derived here and those from the literature, notably the data collected and discussed in RM00. Assuming then that the errors are the same in both sources, we get an estimate of our slope errors, hopefully an upper limit. On the other hand we can consider the internal correlations between the slopes of the various colour-log r relations, specifically Δ_{UB} and others with Δ_{BV}. Figures 5 and 6 show the correlations of the $U-B$ and $V-I$ colour gradients with that in $B-V$. The coefficients of correlation are respectively 0.73 and 0.40. A weighted mean $Gm4$ of the slopes in the 4 colours has also been used as reference instead of Δ_{BV} with analogous results. From the dispersions of such correlations the slope errors can be

Table 8. Probable errors σ_S associated with sky background inaccuracies. Units: magnitude. Estimated errors are the same in $V-R$ as in $B-V$.

Colour	μ_V	$U-B$	$U-V$	$B-V$	$V-I$
1st and 2nd run	23	0.023	0.026	0.008	0.012
id	24	0.058	0.064	0.020	0.030
id	24.5	0.093	0.102	0.032	0.048
3rd run	23	0.017	0.019	0.006	0.010
id	24	0.042	0.048	0.015	0.026
id	24.5	0.067	0.077	0.024	0.041

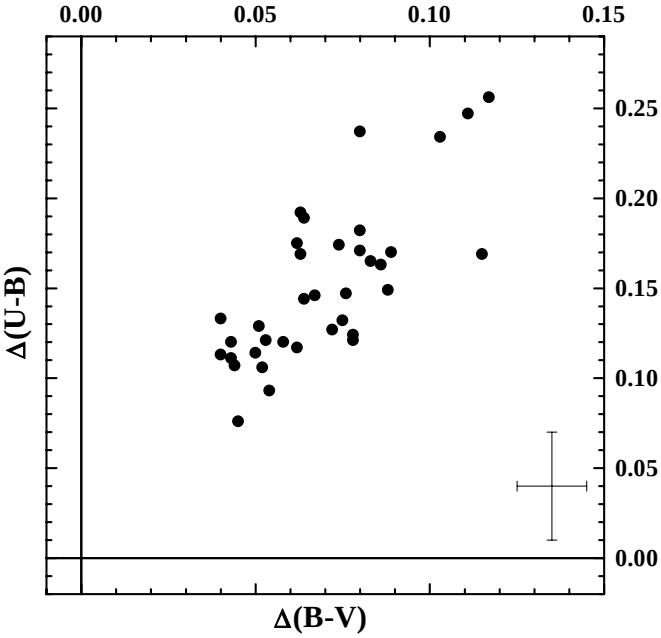

Fig. 5. Correlation between the colour gradients, *with the signs changed.* Abscissae: Δ_{BV}. Ordinates: Δ_{UB}. Compare with the similar diagram in RM00, or with the original correlation diagram between Δ_{BR} and Δ_{UR} in Peletier et al. (1990). The dispersion is clearly reduced here, which can only be attributed to an improved accuracy.

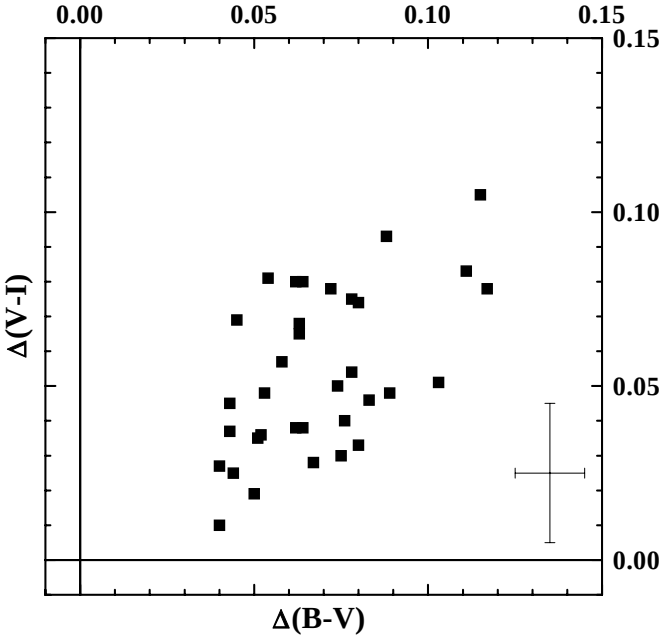

Fig. 6. Correlation between the colour gradients, *with the signs changed*. Abscissae: Δ_{BV}. Ordinates: Δ_{VI}. Here the comparison with similar diagrams in RM00 does not show much increase in the accuracy of the new data.

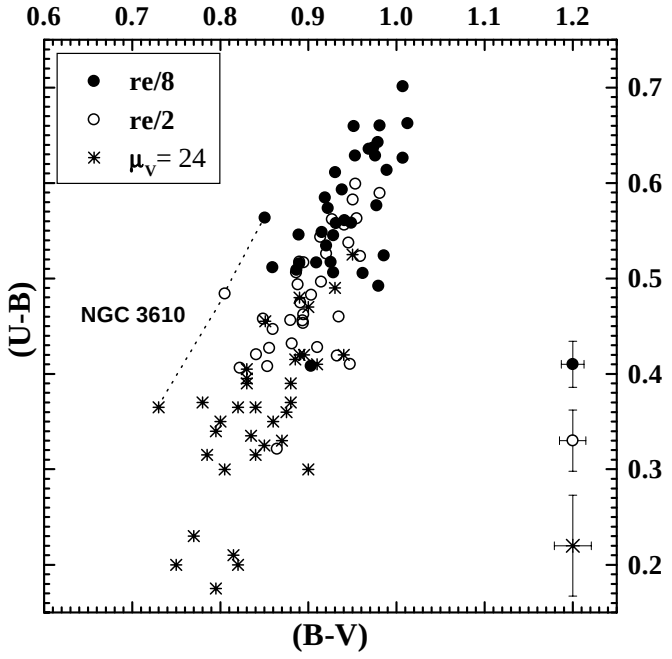

Fig. 7. Colour-colour diagram of $U-B$ against $B-V$: the colours are calculated from the linear representations of Table 9 at the effective radius $r_e/8$ (dots), at $r_e/2$ (circles) and at the outermost range near $\mu_V = 24$ (stars) from Table 11. Although the various symbols refer to widely different regions of the galaxies they define a common relation.

estimated, if the error for the reference $\mathrm{d}B-V/d\log r$ or $Gm4$ is "guessed". The two techniques give results in very good agreement, the internal correlations indicating somewhat smaller errors.
The probable errors of the slope estimates are then 0.03 in U−B or U−V, 0.01 in B−V, 0.015 in V−R or B−R, 0.02 in V−I.

4. Observational results

The available data from the present study are:

1. Table 9, giving for each object the linear representation of the colour-log r relations, i.e. the selected inner and outer radii of the fit, the zero point colour with its probable error σ_C and the slope. The probable errors for the slopes are given above. This table allows easy calculation of the colours at any radius, notably the effective radius r_e and others as considered below.
2. In electronic form only, the tables giving for each galaxy, as a function of the radius r, the V magnitude μ_V and the colours $U-B$, $B-V$, $V-R$, $V-I$. These tables are presently available with the $U-B$ indices as observed, and consistent with Table 9. They will be later made available after correction for suspected effects of PSF far wings (see discussion in 3.2.5).
3. Series of graphs from the above tables, showing the colours as a function of $\log r$ or of μ_V. Examples of these graphs are shown here to illustrate a number of properties of the radius-colour relations.
4. Table 10 gives the "central" colours according to several definitions: we have considered the colours integrated inside the area of radius $r = 3''$, and the colours calculated for $r = 1.5''$ from the linear representations of Table 9. They should be nearly equal if these representations remain valid at small r, which is not always the case: see below for a description of typical deviations.
5. Table 11 collects colours measured at the outermost range of the available data expressed in V magnitude. This gross limit varies between $\mu_V = 23$ (for NGC 4472) and 24.5. It is controlled by the size of the object and the "cleanliness" of the nearby field.

The SA0 galaxies NGC3115, 3607, 4550 and 5866 have been observed with the E-type sample. The corresponding results are given in the tables, but they have been discarded from the discussion.

4.1. Statistical comparison with previous work

– Assuming that colours result only from population variations, "perfect" correlations between zero point colours in different pass-bands are expected. We have compared colour-colour correlations for previous surveys and the present one. For $B-I$ against $B-V$ we find from Goudfrooij et al. (1994) a coefficient of correlation $\rho = 0.61$ (41 objects) compared to $\rho = 0.94$ from Table 9 (37 objects). For $U-R$ against $B-R$ the data of Peletier et al. (1990) (38 objects) give $\rho = 0.58$, while the present data leads to $\rho = 0.94$. The improvement is less if we compare our results with the

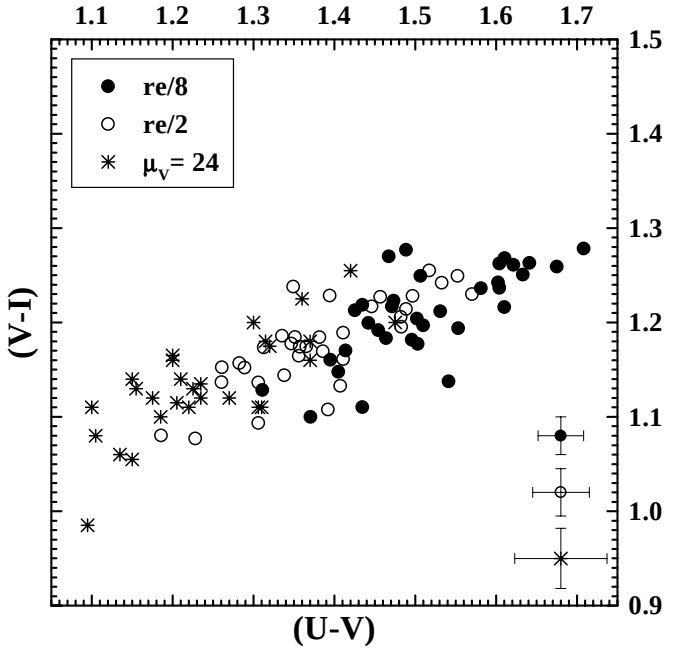

Fig. 8. Colour-colour diagram of $V-I$ against $U-V$: the colours are calculated from the linear representations of Table 9 at the effective radius $r_e/8$ (dots), at $r_e/2$ (circles) and at the outermost range near $\mu_V = 24$ (stars) from Table 11.

discussion in RM00 where the calibration of the available photometry was reconsidered;

– The correlation between colour gradients should also be as good as allowed by errors of measurements. Again we compare the correlation coefficients between gradients from the literature and our results for the same colours. From Goudfrooij et al. (1994), considering the gradient Δ_{BI} against Δ_{BV}, we find $\rho = 0.78$ which is quite good. The result derived from Table 9 is still better, i.e. $\rho = 0.85$. The improvement is more pronounced when the Δ_{UR} against Δ_{BR} correlation is calculated from Peletier et al. (1990): one obtains $\rho = 0.36$ only, instead of $\rho = 0.88$ with our data[2].

– Our colour measurements could be obtained at much lower surface brightness (or larger radii) than in previous work. The present data extend to $23.2 < \mu_V < 25.2$, with a median value near $\mu_V = 24.5$ in all colours. The tables by Goudfrooij et al. (1994), available from CDS Strasbourg, are mostly limited to $\mu_V = 22.75$ in $B-V$ and $\mu_V = 22.25$ in $V-I$ (median values), due to the small fields of the frames, notably in the I band (and probably an ad hoc cut off). Their published graphs generally extend to the same radius in both colours. The tables from Peletier et al. (1990), again at the CDS, extend to $\mu_V = 23.2$ in $B-R$ and $\mu_V = 22.6$ in $U-R$ (mean values) due to a systenatic cut-off at 10% of the sky. The printed tables may be still more severely truncated.

[2] The coefficients of correlation given here are of course different from the previously calculated ones in Sect. 3.2.7.6, which refered to other colours with smaller gradients.

In summary, our colour data generally extends 1.5 to 2 magnitudes deeper than in previous works, so that "external colours" refering to the level $\mu_V = 24.5$ whenever possible, are presented in Table 11 with realistic error estimates.

4.2. Description of isophotal colour profiles

Most of the profiles relating colour to $\log r$, or equivalently to the surface brightness μ_V, are *regular*, meaning that they deviate very little from a straight line in the range of abscissae relevant to the present data, roughly $r > 2''$ and $\mu_V < 24.5$. In this case, the "central colours" integrated within $r < 3''$, and the colours calculated from the linear representation at the average radius of $r = 1.5$, differ very little. Central colour according to these two definitions are given in Table 10: compare Cols. 5 and 6 for $U-V$, and 3 with 7 for $V-R$. Figure 2 gives an example of a set of regular colour profiles for NGC 4473. Of course the linear colour–$\log r$ relation is only approximate and breaks down at small r for all galaxies observed at high resolution. Carollo et al. (1997) obtained $V-i$ maps of a number of E-galaxies from HST frames, disclosing minute colour structures in some cases. In RM99, the CFHT resolution proved sufficient for the detection and classification of $B-R$ central "red peaks". These are smoothed out, at least partly, with the OHP seeing.

Non regular profiles have been observed in the following cases:

1. When an important dust pattern occurs near the center of an object, it produces a central red hump in the colour profile. This is the case for galaxies with the value of 3 for the *dust pattern importance index (DPII)* introduced in RM99, such as NGC 2768, 4125 and 4374, but also for 5813 and 5831. The dust ring of NGC 3607, type SA0, produces noticeable bumps in its colour profiles. Figure 3 gives an example of the colour profiles of such a centrally dusty galaxy, i.e. NGC 4125. In such cases, the integrated colours within $r = 3''$ are redder than the extrapolated colours at $r = 1.5$: this "extra reddening" is smaller in $U-B$ than in other colours. The consideration of the central reddening in $V-R$, a colour nearly insensitive to age-metallicity variations but sensitive to dust, gives a possibility to correct other colours for dust effects. This has been done, in some applications, for galaxies of *DPII* 3.
2. A few objects show a central red hump in some of the colour profiles, specially $U-B$ and also eventually $B-V$. This is the case of NGC 3377, 3379, 3610(?) and 4494. Figure 4 illustrates the case of NGC 3377. For such objects the "extra reddening" defined above is near zero in $V-R$ and $V-I$. It is therefore permitted to attribute it to a metallicity increase rather than to dust.
3. On the contrary, the central colours $U-B$, $B-V$ may be bluer than the extrapolation of the linear portion of the profile. This occurs for objects with larger

than average colour gradients. The best such case is NGC 4636; others are 4283, 4478 and the SA0 4550. An "extra blueing" in $U-V$ is then apparent from the comparison of indices in Cols. 5–6 of Table 10. This is also marginally the case for such giant galaxies as NGC 4406, 4472, 4649: according to RM99 the colour profile of such objects tend to flatten out near the center.

4. NGC 4486 is remarkable in showing a central "blue deep", the $U-B$ colour beeing 0.51 at $r=0$ as compared to 0.72 near $r=6.5''$. This central feature is probably somehow related to the famous non-thermal jet of this galaxy. The jet is of course very conspicuous in $U-B$, with a peak colour near -0.1. Needless to say, both the central "blue deep" and the jet are affected by seeing (and our attempts to correct its effects).

4.3. Correlations of interest

4.3.1. Correlations between colour gradients

The correlations between the various colour gradients have already been noted as useful tools to evaluate the probable errors in gradients. These correlations are displayed in Figs. 5 and 6.

The coefficient of correlation between Δ_{UB} and Δ_{BV} is 0.75; that between Δ_{VI} and Δ_{BV} is only 0.40. For Δ_{VR} it falls to 0.20, because the errors are of the same order of magnitude as the $V-R$ gradients. Imposing regression lines *running through the origin*, the relative slopes are $<\Delta_{UB}/\Delta_{BV}=2.2>$, $<\Delta_{VI}/\Delta_{BV}=0.8>$ and $<\Delta_{VR}/\Delta_{BV}=0.25>$. These relative slopes are in good agreement with the results in RM00, and its conclusion, i.e. the negligible influence of dust upon colour gradient, is confirmed.

The distribution of colour gradients for E-galaxies may be of interest. The following parameters are found: $<\Delta_{UB}>=-0.152$ with $\sigma=0.044$; $<\Delta_{BV}>=-0.070$ with $\sigma=0.021$; $<\Delta_{VR}>=-0.018$ with $\sigma=0.012$; $<\Delta_{VI}>=-0.054$ with $\sigma=0.023$. The dispersions are not much larger than the errors estimated above. The distributions are asymmetric: there are 4 objects with Δ_{BV} larger than $+1.8\sigma$ above the mean, but none at less than the same deviation. These galaxies, with Δ_{BV} clearly steeper than average, by about twice the estimated probable error of measurement, are NGC 4283, 4478, 4564 and 4636, seemingly a random collection.

Remark: an attempt to sort the E-galaxies by flattening as measured in MM94, and to look for some relation to the gradients, lead to negative results. Similarly no significant difference was found between diE and other galaxies.

The SA0 NGC 4550 has quite exceptional gradients in all colours, and an admixture of dust and relatively young stars could be invoked to explain its properties. This object also has very remarkable kinematics, as first described by Rubin et al. (1992); a model has been proposed by Rix et al. (1992). The few other S0s in the present sample are similar to Es with regard to their colour gradients.

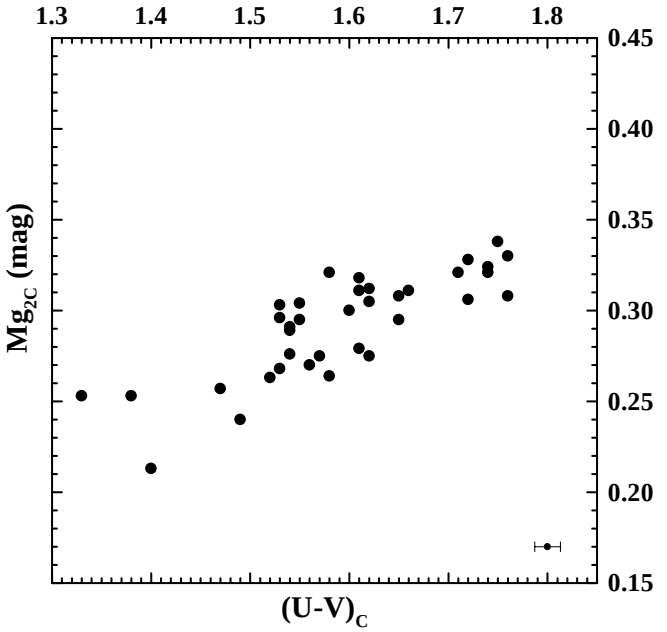

Fig. 9. Correlation between the near center $U-V$ colour in abscissae, and the Mg_2 index from Faber et al. (1989), in ordinates.

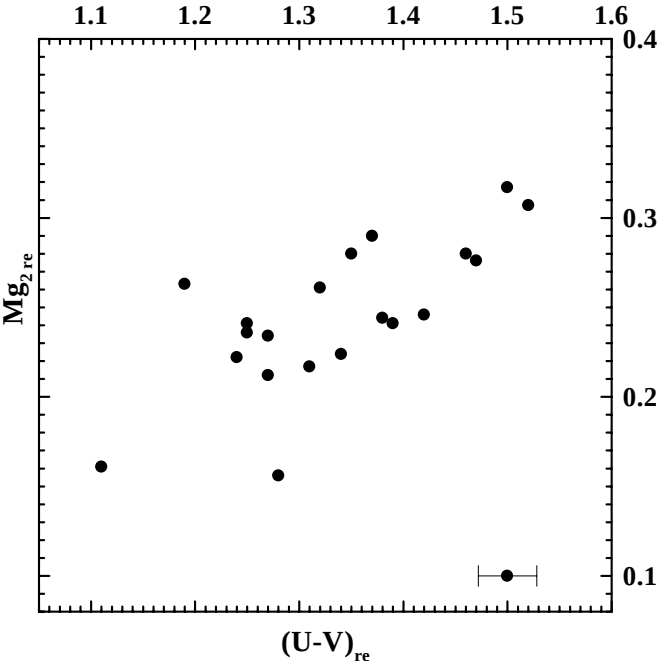

Fig. 10. Correlation between the $U-V$ colour and the Mg_2 index at the effective radius. This index, and the Mg_b one merged in the data, are taken from Kobayashi & Arimoto (1999).

4.3.2. Colour-colour diagrams

Many colour-colour diagrams can be built from the present data. The indices used may be calculated from the linear representations in Table 9 at the effective radius r_e, at a near center position $r_e/8$, and at an intermediate position $r_e/2$. The system of r_e here used is an average of estimates in MM94, Prugniel & Héraudeau (1998), and the RC3. It is satisfactory that the various indices $(B-V)_{r_e}$,

$(B-V)_{r_e/2}$, $(B-V)_{r_e/8}$, define a common diagram with the corresponding $U-B$. This may suggest that a common physical variable controls the variations inside an object, and the object to object changes, of the two colours. Such graphs readily show larger than average calibrations errors: for instance, the $U-B$ colour of NGC 3610 is clearly too red for its $B-V$.

We have also traced colour-colour diagrams for the "central" colours, (Table 10), i.e. integrated in the radius $r < 3''$. They are similar to those traced with the interpolated colours, but with larger dispersions: this is not surprising since the central colours suffer from larger errors (see Sect. 3.2.7).

Finally, one can trace colour-colour diagrams with the "outermost colours" collected in Table 11. They are in fair agreement with the diagrams derived from Table 9, and extend these towards the blue. We show in Fig. 7 a composite colour-colour diagram $U-B$ against $B-V$, using the colours ar $r_e/8$, $r_e/2$ and the outermost range. Similarly Fig. 8 displays the diagram of $V-I$ against $U-V$.

4.3.3. The $U-V$ colour as a metallicity index for ellipticals?

Burstein et al. (1988) showed a correlation between the central Mg_2 index and a global $B-V$ colour measured in a large aperture (see also Bender et al. 1993). This type of correlation is reconsidered here using the $U-V$ colour which is much more sensitive to metallicity than $B-V$, and taking advantage of recent estimates of the Mg_2 index far from center.

Two correlations between the Mg_2 index and $U-V$ are considered in Figs. 9 and 10. The first shows the relation between the two quantities near the galaxy center: the Mg_{2C} index is taken from the tabulation by Faber et al. (1989). The $(U-V)_C$ index is the integrated colour in a circle of radius $r = 3''$. The value for three galaxies with important central dust patterns have been corrected by reference to the central bump in $(V-R)$, a colour sensitive to dust but less so to metallicity changes. The coefficient of correlation reaches 0.825. Taking $(U-V)_C$ as x and Mg_{2C} as y we find the regression $y = 0.221 \pm .027x - 0.061 \pm .003$.

The second, i.e. Fig. 10, displays the correlation between the $U-V$ colour and the Mg_2 index at the effective radius r_e. Mg_{2re} has been taken from Kobayashi & Arimoto (1999) (KA99). To increase the number of data points the Mg_b gradients were introduced, using the linear relation $Mg_b = 15\,Mg_2$ derived from the distribution of the values of both indices in the tables of KA99. The coefficient of correlation still reaches 0.72. Again, with the colour in x and the Mg_{2re} in y we find $y = 0.283 \pm .069x - 0.133 \pm .007$. The difference to the above correlation for central indices is barely significant.

The quality of these correlations proves that both indices are essentially controlled by the same physical variables, and leaves little room for the effects of diffuse dust upon the colours of E-galaxies.

5. Conclusions

New colour-radius relations have been derived for 36 E-type galaxies of the northern Local Supercluster, using $UBVRI$ frames obtained with the 120 cm telescope of the Observatoire de Haute-Provence. Four SA0, i.e. NGC 3115, 3607, 4551 and 5866 were also observed.

We aimed to take advantage of the large field of the camera to observe the galaxies at larger radii than hitherto feasible, and thus improve the accuracy of colour gradients. The availability of the series of aperture photometry in PP88 and PN94 for most of the sample was also considered an asset towards a more coherent system of colours. It appears indeed that *the colour calibrations are improved here compared to previous work*, if this can be judged from the quality of correlations between zero point colours in various surveys (see Sect. 4.1).

Two steps in the reduction procedure were thought significant in improving the quality of colour profiles: the first was the adjustment of the $FWHM$ of the PSFs in a given colour set of 5 frames to the best of the five. This allowed us to get significant colours much closer to the galaxy center than otherwise feasible. The second was a careful "mapping" of the background of each frame, in order to lessen the background fluctuations remaining after the usual flat-fielding procedures. Both these precautions proved successful, and, as a result, the radial range of satisfactory colour measurements was greatly enlarged. Near the galaxy center, it proved feasible to obtain "central colours", i.e. colours integrated in the circle $r = 3''$, in fair agreement with high resolution data (see Sect. 3.2.7.2 and Table 10).

On the other hand, colours could be obtained at much lower surface brightness (or larger radii) than in previous work. Our colour data extend to $23.2 < \mu_V < 25.2$, with a median value near $\mu_V = 24.5$ in all colours. According to the comparisons in Sect. 4.1, this is *1.5 to 2 magnitudes deeper than in previous work*. "External colours", refering to the level $\mu_V = 24.5$ whenever possible, are published for the first time (see Table 11), and may be useful to give some indications about stellar populations at the outskirts of E-galaxies.

On the other hand, the "red halo" effect of the camera was found to give enormous errors in $V-I$ colours and gradients. These were corrected by a rigorous technique, and results in agreement with "classical" data were obtained. Considering the $V-I$ gradients, one is not happy however to introduce in their evaluation, corrections larger than the quantity to be measured! Besides this specific problem of the red halo of thinned CCD, the far wings of the PSFs have been proven in a recent paper (RM01) to have non negligible effects in the gradients of other colours, and also to vary with the age of mirror coatings. It is not impossible that the $U-B$ or $U-V$ gradients given here are overestimated by 15–20%, although they are in excellent

Table 9. Linear representation of colour against $\log r$. Successive columns: NGC No.; Type; $r_{\rm i}$ inner radius of calculation; $r_{\rm o}$ outer radius of calculation; r_0 radius of colour evaluation (in log and "); $U-B$ at r_0 and estimated standard error; Δ_{UB} radial gradient; $B-V$ at r_0 and estimated standard error; Δ_{BV} radial gradient; $V-R$ at r_0 and estimated standard error; Δ_{VR} radial gradient; $V-I$ at r_0 and estimated standard error; Δ_{VI} radial gradient; *du* Dust visibility index (Michard 1999) Notes: 2974: $V-R$ and $V-I$ not measurable; 3193: $V-I$ not measurable.

NGC	Type	$r_{\rm i}$	$r_{\rm o}$	r_0	$U-B$	Δ_{UB}	$B-V$	Δ_{BV}	$V-R$	Δ_{VR}	$V-I$	Δ_{VI}	*du*
2768	diE	10	80	1.467	$0.521 \pm .03$	-0.093	$0.892 \pm .02$	-0.054	$0.536 \pm .02$	-0.012	$1.136 \pm .02$	-0.081	3
2974	diE	8	80	1.404	$0.429 \pm .01$	-0.237	$0.905 \pm .01$	-0.080	-	-	-	-	3
3115	SA0	8	100	1.464	$0.501 \pm .01$	-0.169	$0.912 \pm .01$	-0.069	$0.585 \pm .01$	-0.010	$1.222 \pm .01$	-0.047	0
3193	unE	6	40	1.169	$0.461 \pm .02$	-0.163	$0.924 \pm .01$	-0.086	$0.567 \pm .02$	0.009	-	-	0
3377	diE	8	80	1.399	$0.298 \pm .02$	-0.144	$0.854 \pm .01$	-0.064	$0.510 \pm .01$	-0.014	$1.067 \pm .01$	-0.080	1-
3377	diE	8	80	1.403	$0.289 \pm .02$	-0.170	$0.852 \pm .01$	-0.075	$0.505 \pm .01$	-0.028	$1.074 \pm .01$	-0.105	1-
3379	unE	8	100	1.460	$0.538 \pm .02$	-0.111	$0.918 \pm .01$	-0.043	$0.585 \pm .01$	-0.013	$1.206 \pm .01$	-0.037	1-
3605	boE	4	30	1.043	$0.403 \pm .03$	-0.175	$0.821 \pm .02$	-0.062	$0.517 \pm .02$	-0.014	$1.076 \pm .02$	-0.038	0
3607	SA0	15	100	1.569	$0.451 \pm .02$	-0.111	$0.882 \pm .01$	-0.067	$0.537 \pm .02$	-0.017	$1.149 \pm .02$	-0.046	3
3608	boE	5	50	1.201	$0.415 \pm .03$	-0.189	$0.949 \pm .01$	-0.064	$0.542 \pm .01$	-0.020	$1.175 \pm .01$	-0.038	1-
3610	diE	4	50	1.159	$0.448 \pm .04$	-0.132	$0.785 \pm .01$	-0.075	$0.503 \pm .01$	0.003	$1.144 \pm .02$	-0.030	0
3613	diE	6	60	1.287	$0.470 \pm .03$	-0.174	$0.875 \pm .02$	-0.074	$0.533 \pm .04$	-0.018	$1.100 \pm .04$	-0.050	1-
3640	boE	5	60	1.266	$0.455 \pm .03$	-0.120	$0.892 \pm .02$	-0.043	$0.544 \pm .02$	-0.012	$1.162 \pm .03$	-0.045	0
3872	diEp	5	60	1.202	$0.506 \pm .03$	-0.127	$0.928 \pm .02$	-0.072	$0.571 \pm .01$	-0.005	$1.176 \pm .02$	-0.078	0
4125	diE	10	80	1.445	$0.497 \pm .03$	-0.165	$0.890 \pm .02$	-0.083	$0.568 \pm .03$	-0.011	$1.183 \pm .03$	-0.046	3
4261	boE	5	80	1.320	$0.588 \pm .03$	-0.170	$0.948 \pm .01$	-0.089	$0.585 \pm .01$	-0.014	$1.246 \pm .02$	-0.048	1-
4278	diE	10	60	1.361	$0.408 \pm .02$	-0.149	$0.845 \pm .01$	-0.088	$0.554 \pm .03$	-0.031	$1.145 \pm .03$	-0.093	?
4283	unE	5	30	1.080	$0.410 \pm .02$	-0.256	$0.870 \pm .01$	-0.117	$0.533 \pm .02$	-0.040	$1.147 \pm .02$	-0.078	0
4365	boE	5	120	1.430	$0.552 \pm .02$	-0.120	$0.939 \pm .01$	-0.058	$0.588 \pm .01$	-0.011	$1.226 \pm .02$	-0.057	0
4374	unE	8	80	1.394	$0.497 \pm .03$	-0.107	$0.915 \pm .01$	-0.044	$0.565 \pm .02$	-0.020	$1.189 \pm .02$	-0.025	3
4387	boE	5	30	1.102	$0.431 \pm .02$	-0.106	$0.883 \pm .01$	-0.052	$0.565 \pm .01$	-0.028	$1.170 \pm .02$	-0.036	0
4406	boE	5	80	1.312	$0.463 \pm .02$	-0.121	$0.961 \pm .01$	-0.078	$0.561 \pm .01$	-0.018	$1.204 \pm .01$	-0.054	0
4472	unE	5	150	1.510	$0.590 \pm .02$	-0.133	$0.963 \pm .01$	-0.040	$0.592 \pm .01$	-0.005	$1.257 \pm .01$	-0.010	0
4473	diE	5	80	1.310	$0.423 \pm .03$	-0.169	$0.881 \pm .01$	-0.063	$0.598 \pm .01$	-0.021	$1.225 \pm .01$	-0.065	0
4478	boE	6	50	1.286	$0.300 \pm .02$	-0.234	$0.806 \pm .01$	-0.103	$0.525 \pm .01$	-0.023	$1.129 \pm .01$	-0.051	0
4486	unE	10	120	1.559	$0.566 \pm .02$	-0.192	$0.921 \pm .01$	-0.063	$0.601 \pm .01$	-0.019	$1.235 \pm .02$	-0.068	0
4494	unE	5	80	1.340	$0.452 \pm .03$	-0.114	$0.862 \pm .01$	-0.050	$0.518 \pm .02$	-0.016	$1.137 \pm .02$	-0.019	?
4550	SA0	5	40	1.199	$0.260 \pm .02$	-0.252	$0.826 \pm .01$	-0.196	$0.511 \pm .01$	-0.108	$1.119 \pm .02$	-0.185	0
4551	boE	5	40	1.184	$0.475 \pm .02$	-0.113	$0.880 \pm .01$	-0.040	$0.525 \pm .02$	-0.014	$1.151 \pm .02$	-0.027	0
4552	unE	5	100	1.366	$0.489 \pm .01$	-0.171	$0.943 \pm .01$	-0.080	$0.546 \pm .01$	-0.035	$1.191 \pm .02$	-0.074	0
4564	diE	5	50	1.233	$0.369 \pm .02$	-0.247	$0.884 \pm .01$	-0.111	$0.545 \pm .01$	-0.024	$1.124 \pm .02$	-0.083	1-
4621	diE	5	80	1.327	$0.522 \pm .02$	-0.182	$0.919 \pm .01$	-0.080	$0.584 \pm .01$	-0.004	$1.216 \pm .02$	-0.033	0
4636	unE	7	100	1.416	$0.495 \pm .02$	-0.169	$0.906 \pm .02$	-0.115	$0.562 \pm .02$	-0.034	$1.185 \pm .03$	-0.105	?
4649	unE	5	150	1.515	$0.592 \pm .01$	-0.121	$0.982 \pm .01$	-0.053	$0.571 \pm .01$	-0.036	$1.231 \pm .02$	-0.048	0
5322	boE	5	80	1.313	$0.445 \pm .03$	-0.146	$0.843 \pm .02$	-0.067	$0.530 \pm .02$	-0.001	$1.091 \pm .03$	-0.028	0
5576	boEp	5	60	1.216	$0.382 \pm .02$	-0.147	$0.821 \pm .01$	-0.076	$0.521 \pm .01$	-0.003	$1.126 \pm .01$	-0.040	0
5813	unE	5	60	1.229	$0.477 \pm .01$	-0.076	$0.945 \pm .01$	-0.045	$0.589 \pm .01$	-0.022	$1.244 \pm .02$	-0.069	1
5831	diE	4	50	1.175	$0.423 \pm .03$	-0.124	$0.876 \pm .02$	-0.078	$0.515 \pm .02$	-0.040	$1.168 \pm .02$	-0.075	?
5846	unE	5	100	1.407	$0.594 \pm .02$	-0.129	$0.955 \pm .02$	-0.051	$0.586 \pm .02$	-0.016	$1.245 \pm .02$	-0.035	0
5866	SA0	15	110	1.612	$0.367 \pm .02$	-0.190	$0.819 \pm .01$	-0.100	$0.537 \pm .01$	-0.048	$1.095 \pm .02$	-0.042	3+
5982	boE	8	100	1.447	$0.431 \pm .02$	-0.117	$0.868 \pm .02$	-0.062	$0.522 \pm .02$	-0.043	$1.145 \pm .02$	-0.080	?

statistical agreement with the well-known work of Peletier et al. (1990).

Various colour gradients against $\log r$ for a given object are well correlated, generally better than in previous work (see statistics in Sect. 4.1), which is interpreted as due to smaller measuring errors, notably in $U-B$. These improvements in accuracy did not bring out any obvious correlation between gradients and other galaxy properties.

Table 10. Columns 1 to 5: integrated colours within a radius $r = 3''$, i.e. UB_3, BV_3 , VR_3 , VI_3, UV_3; Col. 6: $UV_{1.5}$ $U-V$ colour at $r = 1.5''$ calculated from Table 9. Column 7 $VR_{1.5}$ $V-R$ colour at $r = 1.5''$.

NGC	UB_3	BV_3	VR_3	VI_3	UV_3	$UV_{1.5}$	$VR_{1.5}$
2768	0.72	1.04	0.61	1.28	1.76	1.60	0.55
2974	0.58	1.03	-	-	1.60	1.72	0.00
3115	0.68	1.03	0.60	1.25	1.72	1.72	0.60
3193	0.60	0.96	0.65	1.32	1.55	1.63	0.58
3377	0.56	0.98	0.54	1.14	1.54	1.41	0.53
3377	0.60	0.98	0.55	1.14	1.57	1.44	0.54
3379	0.72	1.03	0.60	1.23	1.76	1.65	0.60
3605	0.50	0.90	0.57	1.13	1.40	1.43	0.53
3607	0.63	1.04	0.64	1.31	1.67	1.69	0.56
3608	0.61	1.01	0.60	1.24	1.62	1.62	0.56
3610	0.60	0.88	0.55	1.07	1.47	1.44	0.50
3613	0.63	0.98	0.57	1.21	1.61	1.63	0.53
3640	0.58	0.94	0.59	1.21	1.52	1.52	0.56
3872	0.63	0.98	0.62	1.22	1.61	1.64	0.58
4125	0.73	1.06	0.65	1.29	1.79	1.64	0.63
4261	0.73	1.03	0.61	1.29	1.76	1.83	0.60
4278	0.55	0.99	0.60	1.21	1.54	1.53	0.64
4283	0.56	0.96	0.60	1.18	1.53	1.62	0.57
4365	0.71	1.04	0.61	1.28	1.74	1.71	0.64
4374	0.63	1.03	0.64	1.30	1.66	1.60	0.59
4387	0.51	0.98	0.57	1.16	1.49	1.46	0.59
4406	0.59	1.02	0.57	1.26	1.61	1.65	0.58
4472	0.70	1.02	0.61	1.29	1.72	1.78	0.60
4473	0.60	0.95	0.64	1.29	1.55	1.57	0.62
4478	0.45	0.89	0.55	1.17	1.33	1.48	0.55
4486	0.55	0.98	0.63	1.26	1.53	1.84	0.63
4494	0.65	0.93	0.57	1.21	1.57	1.50	0.54
4550	0.39	0.95	0.58	1.22	1.34	1.54	0.62
4551	0.59	0.99	0.58	1.23	1.58	1.51	0.54
4552	0.67	1.07	0.61	1.29	1.74	1.73	0.59
4564	0.63	0.95	0.61	1.19	1.58	1.63	0.57
4621	0.72	1.00	0.63	1.27	1.72	1.74	0.59
4636	0.67	1.00	0.60	1.29	1.66	1.79	0.61
4649	0.71	1.04	0.62	1.29	1.75	1.81	0.62
5322	0.62	0.91	0.62	1.21	1.54	1.53	0.53
5576	0.53	0.85	0.58	1.17	1.38	1.43	0.53
5813	0.64	1.01	0.65	1.33	1.65	1.55	0.61
5831	0.59	0.95	0.57	1.25	1.54	1.50	0.55
5846	0.69	1.01	0.62	1.28	1.71	1.77	0.61
5866	-	-	-	-	-	1.60	0.61
5982	0.59	0.94	0.54	1.18	1.53	1.53	0.58

Table 11. "External colours" measured in the outermost range of the data. Successive columns: μ_V V surface brightness of measurement, a range of 0.5 mag centered at the quoted μ_V beeing used. Columns 2–5: $U-B$, $B-V$, $V-R$, $V-I$ respectively with estimated errors. These are the same in $V-R$ as in $B-V$.

NGC	μ_V	$U-B$	$B-V$	$V-R$	$V-I$
2768	24.25	$0.455 \pm .06$	$0.851 \pm .02$	0.530	$1.110 \pm .04$
2974	id	$0.335 \pm .06$	$0.835 \pm .03$	0.000	$0.000 \pm .00$
3115	id	$0.365 \pm .05$	$0.855 \pm .02$	0.580	$1.180 \pm .03$
3193	23.5	$0.370 \pm .04$	$0.880 \pm .02$	0.000	$0.000 \pm .00$
3377	24.5	$0.210 \pm .06$	$0.815 \pm .02$	0.505	$1.000 \pm .03$
3377	24.25	$0.175 \pm .05$	$0.795 \pm .02$	0.480	$0.950 \pm .03$
3379	24.0	$0.480 \pm .04$	$0.890 \pm .02$	0.575	$1.160 \pm .03$
3605	23.5	$0.340 \pm .03$	$0.795 \pm .02$	0.510	$1.060 \pm .02$
3607	24.25	$0.370 \pm .07$	$0.845 \pm .03$	0.530	$1.130 \pm .04$
3608	23.75	$0.300 \pm .05$	$0.900 \pm .02$	0.525	$1.165 \pm .03$
3610	24.25	$0.365 \pm .05$	$0.730 \pm .02$	0.510	$0.985 \pm .04$
3613	24.5	$0.395 \pm .07$	$0.830 \pm .02$	0.500	$1.130 \pm .04$
3640	23.5	$0.360 \pm .04$	$0.875 \pm .02$	0.540	$1.135 \pm .03$
3872	24.5	$0.420 \pm .07$	$0.890 \pm .03$	0.555	$1.110 \pm .05$
4125	23.5	$0.405 \pm .03$	$0.830 \pm .01$	0.550	$1.120 \pm .02$
4278	23.5	$0.350 \pm .04$	$0.800 \pm .02$	0.530	$1.055 \pm .03$
4283	23.75	$0.300 \pm .05$	$0.805 \pm .02$	0.510	$1.080 \pm .03$
4365	24.	$0.470 \pm .04$	$0.900 \pm .02$	0.585	$1.180 \pm .03$
4374	23.25	$0.420 \pm .03$	$0.895 \pm .01$	0.545	$1.180 \pm .03$
4387	24.5	$0.350 \pm .08$	$0.860 \pm .03$	0.550	$1.140 \pm .05$
4406	23.25	$0.330 \pm .04$	$0.870 \pm .02$	0.565	$1.160 \pm .03$
4472	23.	$0.490 \pm .03$	$0.930 \pm .01$	0.590	$1.255 \pm .02$
4473	24.5	$0.315 \pm .08$	$0.840 \pm .03$	0.575	$1.130 \pm .05$
4478	24.	$0.200 \pm .04$	$0.750 \pm .02$	0.490	$1.090 \pm .03$
4486	23.5	$0.415 \pm .03$	$0.885 \pm .02$	0.590	$1.200 \pm .03$
4494	24.5	$0.390 \pm .08$	$0.830 \pm .03$	0.500	$1.110 \pm .05$
4550	24.0	$0.120 \pm .06$	$0.700 \pm .02$	0.470	$1.010 \pm .03$
4551	24.5	$0.325 \pm .07$	$0.850 \pm .03$	0.520	$1.120 \pm .04$
4552	24.	$0.390 \pm .06$	$0.880 \pm .02$	0.515	$1.120 \pm .03$
4564	24.5	$0.200 \pm .07$	$0.820 \pm .02$	0.530	$1.020 \pm .03$
4621	24.	$0.390 \pm .06$	$0.370 \pm .02$	0.565	$1.175 \pm .03$
4636	23.5	$0.370 \pm .03$	$0.780 \pm .02$	0.510	$1.140 \pm .03$
4649	23.5	$0.525 \pm .04$	$0.950 \pm .02$	0.540	$1.200 \pm .03$
5322	24.25	$0.315 \pm .07$	$0.785 \pm .03$	0.520	$1.110 \pm .04$
5576	23.75	$0.230 \pm .05$	$0.770 \pm .02$	0.525	$1.085 \pm .03$
5813	24.	$0.410 \pm .06$	$0.910 \pm .02$	0.575	$1.175 \pm .03$
5831	23.	$0.365 \pm .06$	$0.940 \pm .02$	0.580	$1.225 \pm .03$
5866	24.5	$0.270 \pm .08$	$0.840 \pm .02$	0.495	$1.115 \pm .04$
5846	24.	$0.420 \pm .06$	$0.940 \pm .02$	0.580	$1.225 \pm .03$
5866	24.5	$0.270 \pm .08$	$0.775 \pm .03$	0.505	$1.075 \pm .05$
5982	24.25	$0.365 \pm .07$	$0.820 \pm .03$	0.500	$1.100 \pm .04$

A few galaxies have exceptionally steep colour gradients (nearly at 2σ) without sharing other properties.

Colour-colour relations can be built from the present data for several locations in galaxies, such as near center, various fractions of the effective radius r_e, or the "outermost" measured range around $\mu_V = 24$. All these diagrams overlap to form a single stripe with moderate scatter (except for one rather obvious calibration error?). These might prove useful to test theories of old stellar populations and of their host galaxies. Colour-colour diagrams based upon integrated colours have already been used for this purpose (Worthey 1994).

The $U-B$ or $U-V$ colours correlate very well with the Mg_2 index, both near the galaxy center and at the effective radius r_e. This seems to rule out any large influence of diffuse dust in the colours and colour gradients in

E-galaxies. This was considered likely by Witt et al. (1992) and discussed by Wise & Silva (1996) with inconclusive results. Previous arguments against such an influence were presented in RM00: they were based upon the relative average values of the gradients in various colours, and are reinforced in the present work, since the mean gradients are nearly unchanged, and their errors lessened.

It is well known that, for single-burst stellar populations, colours and line indices depend both on the metallicity and on the age of the system (Worthey 1994; Borges et al. 1995). However, E-galaxies are constituted by a population mix, having age and metallicity distributions which reflect their star formation histories. Therefore a colour-metallicity calibration requires the use of models able to provide those distributions and, consequently, the integrated colours along the galaxy lifetime. Such a calibration will be presented in Paper II.

Acknowledgements. TPI acknowledges a Fapesp pos-doc fellowship No. 97/13083-7.

References

Bender, R., & Möllenhof, C. 1987, A&A, 177, 71
Bender, R., Burstein, D., & Faber, S. M. 1993, ApJ, 411, 153
Borges, A. C., Idiart, T. P., de Freitas Pacheco, J. A., et al. 1995, AJ, 110, 2408
Burstein, D., Davies, R. C., Dressler, A., et al. 1988, in Towards Understanding Galaxies at Large Redshift, ed. R. G. Kron, & A. Renzini (Kluwer, Dordrecht)
Carter, D. 1978, MNRAS, 182, 797
de Vaucouleurs, G., de Vaucouleurs, A., Corwin, H. G. Jr., et al. 1991, Third Reference Catalogue of Bright Galaxies (Springer, New York)
Faber, S. M., Wegner, G., Burstein, D., et al. 1989, ApJS, 69, 763
Franx, M., Illingworth, G., & Heckman, T. 1989, AJ, 98, 538 (FIH)
Goudfrooij, P., Hansen, L., Jorgensen, H. E., et al. 1994, A&AS, 104, 179
Michard, R., & Marchal, J. 1994, A&AS, 105, 481 (MM94)
Michard, R. 1999, A&AS, 137, 245 (RM99)
Michard, R. 2000, A&A, 360, 85 (RM00)
Michard, R. 2001, A&A, in press (RM01)
Peletier, R. F., Davies, R. L., Illingworth, G. D., et al. 1990, AJ, 100, 1091
Poulain, P. 1988, A&AS, 72, 215
Poulain, P., & Nieto, J. L. 1994, A&AS, 103, 573
Prugniel, P., & Héraudeau, P. 1998, A&AS, 128, 299
Rubin, V. C., Graham, J. A., & Kenney, J. D. P. 1992, ApJ, 394, L9
Rix, H. W., Franx, M., & Fisher, D. 1992, ApJ, 400, L5
Trager, S. C., Faber, S. M., Worthey, G., et al. 2000, ApJ, 119, 1645
Vigroux, L., Souviron, J., Lachieze-Rey, M., et al. 1988, A&AS, 73, 1
Wise, M. W., & Silva, D. R. 1996, ApJ, 461, 155
Witt, A., Thronson, H. A. Jr., & Capuano, J. M. 1992, ApJ, 393, 611
Worthey, G. 1994, ApJS, 95, 107